

# Role of Anisotropy and Refractive Index in Scattering and Whiteness Optimization

Gianni Jacucci,\* Jacopo Bertolotti, and Silvia Vignolini\*

The ability to manipulate light–matter interaction to tailor the scattering properties of materials is crucial to many aspects of everyday life, from paints to lighting, and to many fundamental concepts in disordered photonics. Light transport and scattering in a granular disordered medium are dictated by the spatial distribution (structure factor) and the scattering properties (form factor and refractive index) of its building blocks. As yet, however, the importance of anisotropy in such systems has not been considered. Here, a systematic numerical survey that disentangles and quantifies the role of different kinds and degrees of anisotropy in scattering optimization is reported. It is shown that ensembles of uncorrelated, anisotropic particles with nematic ordering enables to increase by 20% the reflectance of low-refractive index media ( $n = 1.55$ ), using only three-quarters of material compared to their isotropic counterpart. Additionally, these systems exhibit a whiteness comparable to conventionally used high-refractive index media, e.g.,  $\text{TiO}_2$  ( $n = 2.60$ ). Therefore, the findings not only provide an understanding of the role of anisotropy in scattering optimization, but they also showcase a novel strategy to replace inorganic white enhancers with sustainable and biocompatible products made of biopolymers.

(structure factor) and their specific characteristics (form factor and refractive index).<sup>[1–4]</sup> Therefore, most efforts to control light propagation in random systems have been focused upon the optimization of isotropic spatial correlations in high-refractive index systems. These studies had a remarkable impact in many fundamental<sup>[5–16]</sup> and applied phenomena.<sup>[17–21]</sup>

However, the role of anisotropy in multiple scattering systems has been overlooked. In fact, despite the well-known analytical solution for the single scattering,<sup>[4,22]</sup> the response of an ensemble of randomly arranged anisotropic particles has not been theoretically investigated. The same is valid for the presence of anisotropic structural correlations. Similarly, recent experimental works focused on the fabrication and optical characterization of anisotropic, disordered materials but without proving the role of anisotropy in scattering optimization.<sup>[23–30]</sup>

## 1. Introduction

Scattering optimization plays an important role in many aspects of our daily life. In particular, for the production of bright-white materials, commonly used as white or color enhancers in cosmetics, food colorings, and standard paints. Therefore, the development of strategies to increase scattering strength of materials is of crucial importance to reduce the consumption of starting resources and consequently the overall production costs.

The scattering strength of a random system depends on the interplay between the spatial distribution of its components

Here, we study the effect of structural and single-particle anisotropy on the opacity of a material and identify the criteria to improve scattering over a large parameter space, including filling fraction and refractive index. Our work proves that ensembles of uncorrelated, anisotropic particles outperform their isotropic counterpart both for low- and high-refractive indices. In addition, anisotropic, low-refractive index systems not only require a lower amount of material to maximize scattering than isotropic media, but they also exhibit a whiteness comparable to those of high-refractive index materials.

Our results showcase how to exploit natural resources (e.g., biopolymers) to replace commercially available white enhancers, made from inorganic high-refractive materials (e.g.,  $\text{TiO}_2$ ), which have recently raised safety concerns.<sup>[31,32]</sup> Moreover, our work unveils why anisotropy is an evolutionary-chosen mechanism to optimize scattering in biological systems.

G. Jacucci, Dr. S. Vignolini  
Department of Chemistry  
University of Cambridge  
Lensfield Road, Cambridge CB2 1EW, UK  
E-mail: gj232@cam.ac.uk; sv319@cam.ac.uk

Dr. J. Bertolotti  
Department of Physics and Astronomy  
University of Exeter  
Stocker Road, Exeter EX4 4QL, UK

 The ORCID identification number(s) for the author(s) of this article can be found under <https://doi.org/10.1002/adom.201900980>.

© 2019 The Authors. Published by WILEY-VCH Verlag GmbH & Co. KGaA, Weinheim. This is an open access article under the terms of the Creative Commons Attribution License, which permits use, distribution and reproduction in any medium, provided the original work is properly cited.

DOI: 10.1002/adom.201900980

## 2. Results and Discussion

To establish a comparison between different disordered materials, we numerically investigated the optical properties of 2D media (see Sections S1 and S2 in the Supporting Information). Exploiting a 2D numerical approach allows to independently vary the structural and form factors of a system, and therefore to disentangle their role in scattering optimization, while avoiding computational burden. In particular, we systematically

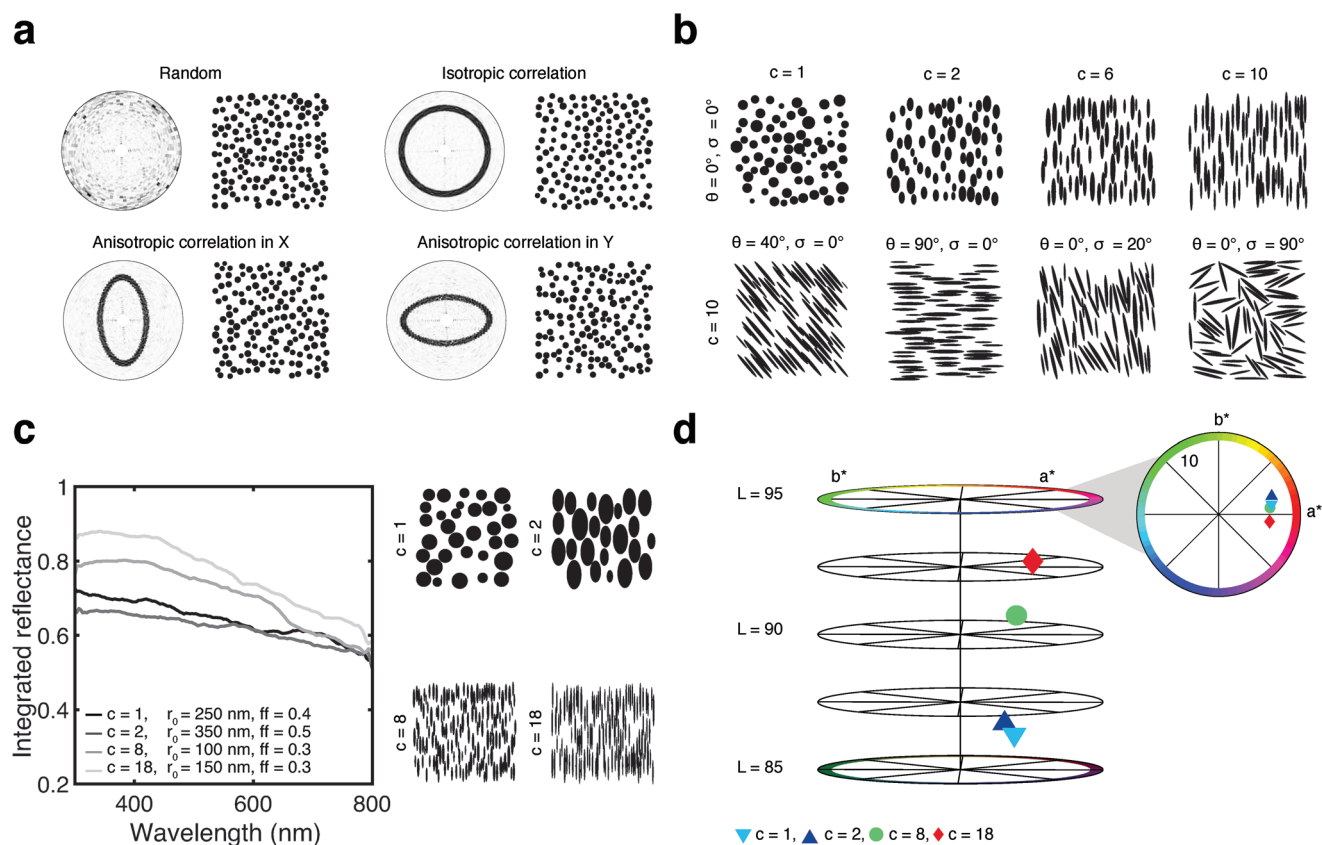


**Figure 1.** Numerical generated 2D systems with various kinds and degrees of anisotropy: a) Ensembles of isotropic particles with different structural correlations. Each structure factor is represented in polar coordinates and the anisotropy direction is defined as the short axis of  $S(\mathbf{q})$ . The peak at  $\mathbf{q} = 0$ , due to the finite size of the simulated structures, was removed. b) Ensembles of uncorrelated particles with varying aspect ratio ( $c$ ) and orientation (sampled from a Gaussian distribution with mean  $\theta$  and standard distribution  $\sigma$ ). c) Simulated optical response of structures with the best filling fraction ( $ff$ ) and aspect ratio for different size of the particles ( $r_0$ ).  $r_0$  corresponds to the radius of the particles at  $c = 1$ . The best reflectance was obtained for anisotropic scatterers ( $c = 10$ ) and a low filling fraction ( $ff = 0.3$ ). All the structures have a thickness of  $10 \mu\text{m}$  and a 20% polydispersity in the size distribution of their building blocks (Section S3, Supporting Information), whose refractive index is  $n = 1.55$ . d) Polar plot showing the CIELAB color space coordinates of the spectra in panel (c).

studied systems with varying degrees and types of anisotropy, namely, structural anisotropy (Figure 1a) and form anisotropy (Figure 1b) for two values of refractive index ( $n = 1.55$  for biopolymer<sup>[33]</sup> and  $n = 2.60$  for the rutile phase of  $\text{TiO}_2$ <sup>[34]</sup>).

The structural anisotropy of a system can be quantitatively described by the structure factor ( $S(\mathbf{q})$ ), which is related to the Fourier transform of the positions of its building blocks and it is defined as

$$S(\mathbf{q}) = \frac{1}{N} \left\langle \sum_{i,j=1}^N e^{-i\mathbf{q} \cdot (\mathbf{r}_i - \mathbf{r}_j)} \right\rangle \quad (1)$$

where  $\mathbf{q}$  is the wave vector,  $N$  is the total number of particles,  $\mathbf{r}$  is the position of the particle, and  $\langle \dots \rangle$  denotes ensemble average. An anisotropic  $S(\mathbf{q})$  translates into an anisotropic average distance between the scattering elements. Figure 1a shows four different ensembles of isotropic particles (disks) with different structural correlations and their respective structure factors.

Similarly, the form factor ( $P(\mathbf{q})$ ) represents the Fourier transform of the shape of a particle and, in two dimensions, is defined as

$$P(\mathbf{q}) = \int_{A_p} e^{-i\mathbf{q} \cdot \mathbf{r}} d\mathbf{r} \quad (2)$$

where  $A_p$  is the area of the particle. In Figure 1b, the form anisotropy is classified in terms of aspect ratio ( $c$ ) and orientation of the particles (with  $\theta$  angle between the incoming light and the direction perpendicular to the long axis of the particles). Structures with different degree of alignment were generated by sampling  $\theta$  from a Gaussian distribution with standard deviation  $\sigma$ .

By changing the degree and type of anisotropy for different size of the particles ( $r_0$ , i.e., the radius of the isotropic object with equivalent area) and filling fraction ( $ff$ ), we identified the set of structural and single-particle parameters that maximize the reflected intensity. The results for  $n = 1.55$  are summarized in Figure 1c. In particular, ensembles of anisotropic particles exhibit a broadband increase in reflectance of almost 20% compared to isotropic systems, while requiring 25% less material to maximize scattering (from  $ff = 0.4$  to  $ff = 0.3$ ).

To compare different samples in terms of whiteness (broadband scattering), the simulated spectra were mapped to the CIELAB color space (see Section S4 in the Supporting

**Table 1.** Parameters that exhibit the highest whiteness ( $W$ ) for particles with different sizes ( $r_0$ , i.e., the radius at  $c = 1$ ) and refractive index ( $n$ ). Anisotropic ( $c = 18$ ), low-refractive index particles show a whiteness comparable to that of high-refractive index particles.

$n$	$r_0$ [nm]	$c$	ff	$W$
1.55	100	8	0.3	88
1.55	150	18	0.3	90
1.55	250	1	0.4	85
1.55	350	2	0.5	85
2.60	50	500	0.4	91
2.60	100	1	0.3	90

Information).<sup>[35,36]</sup> CIELAB is a euclidian space, allowing an intuitive definition of whiteness ( $W$ ) as<sup>[37]</sup>

$$W = 100 - |\mathbf{X}_w - \mathbf{X}_m| \quad (3)$$

where  $|\dots|$  denotes the euclidian distance,  $\mathbf{X}_w = \{100, 0, 0\}$ , and  $\mathbf{X}_m$  are the CIELAB coordinates of a perfect broadband diffuser (also known as white point) and of the material of interest, respectively. Figure 1d shows the color space representation of the spectra in Figure 1c. According to **Table 1**, low-refractive index ( $n = 1.55$ ) particles with  $c = 18$  not only outperform their isotropic counterpart but they also exhibit a whiteness comparable to that of high-refractive index ( $n = 2.60$ ) scattering materials. The optimal value of aspect ratio we obtained is in good agreement with the one reported for the *Cyphochilus* beetle, where  $c \approx 10$ .<sup>[26]</sup> However, it is important to note that ref. [26] does not claim that the size of the fibrils in the biological network is optimized.

Interestingly, for high-refractive index, anisotropic systems outperform ensembles of optimized isotropic particles only for aspect ratios larger than 40 (more details in Section S5, Supporting Information). The predicted optimal values of radius ( $r_0 = 100$ nm) and filling fraction (ff = 0.3) for isotropic systems with  $n = 2.60$  are in agreement with those reported in theoretical and experimental studies regarding scattering optimization for titanium-dioxide particles.<sup>[21,38–41]</sup> Moreover, Figure S2d in the Supporting Information shows that, after exhibiting a strong growth in function of the aspect ratio, between  $c = 400$  and  $c = 1400$ , the integrated reflectance shows a less marked dependence on  $c$ , with a maximum value at  $c = 500$ . At even higher aspect ratios, the systems approach the 1D limit (i.e., particles as long as the lateral dimension of the material) where a further increase in the integrated reflectance is expected.<sup>[42,43]</sup>

More importantly, the difference in integrated reflectance between the ensembles of isotropic and anisotropic particles cannot be explained only in terms of single scattering (Section S6, Supporting Information). Indeed, as depicted in Figure S3a,b in the Supporting Information, isotropic particles have a larger scattering efficiency over the visible than anisotropic scatterers. However, Figure S3b–d in the Supporting Information shows that the angular distribution of light scattered by anisotropic particles exhibits a lobe both in the backward and forward directions, whereas their isotropic counterparts scatter mainly forward. Therefore, our results suggest

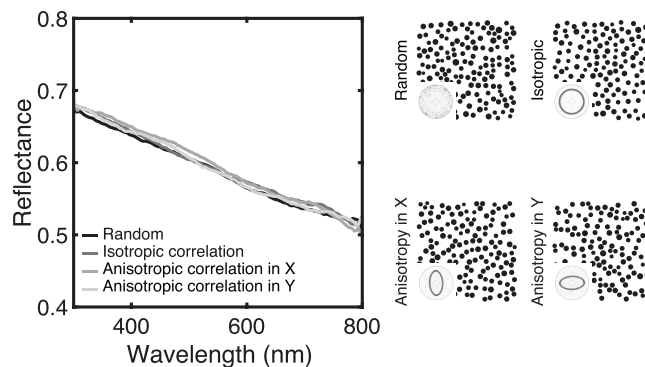


**Figure 2.** Simulated optical response for systems with different structural anisotropy. The structure factor relative to each ensemble of particles is shown as an inset. An anisotropic  $S(\mathbf{q})$  does not affect the broadband reflectivity of a system. All the simulated structures have a thickness of  $10 \mu\text{m}$ , ff = 0.3, building blocks with  $n = 1.55$ , and  $r = 250$  nm.

that such a difference must play a more important role in the multiple scattering than the single-particle scattering efficiency.

To disentangle the role of structural and form anisotropy in the scattering efficiency, we first compare the effect of structural correlations on the optical properties of disordered systems consisting of isotropic particles. The size of the particles was sampled from a Gaussian distribution with mean  $r = 250$  nm, which is the optimal value for particles with  $c = 1$  and  $n = 1.55$  (see Table S2 in the Supporting Information). **Figure 2** shows that anisotropic correlations do not alter the spectral response of a system. For high-refractive index materials ( $n = 2.60$ ), a small increase in the reflectivity is observed in the presence of structural correlations, similar to what is reported in ref. [21], and introducing an anisotropic  $S(\mathbf{q})$  did not affect in a significant way the optical properties (see Section S7 in the Supporting Information).

Conversely, a change in the form factor of the particles drastically affects the response of a system. In particular, different kinds and levels of form anisotropy were studied separately: First, to identify the optimal value of  $c$ , particles with same area, same orientation ( $\theta = \sigma = 0$ ) but different aspect ratio were considered (**Figure 3**). Second, ensembles of particles with same  $c$  were compared in function of their degree of alignment (**Figure 4**).

Figure 3a shows that tuning the aspect ratio of the particles leads to a marked change in the scattering efficiency of a medium, with a maximum at  $c = 18$ .  $c$  not only determines the brightness of a sample, but it also strongly affects its color saturation. The large range of aspect ratios we studied models both particle- and fibril/fiber-based materials.

Additionally, once understood which aspect ratio maximizes the whiteness (see Table S2 in the Supporting Information), the number of particles in the system was varied to optimize the filling fraction. Figure 3b shows that while the filling fraction has a strong influence in determining the reflectance of a sample, the color saturation is not strongly dependent on ff. The results in Figure 3 refer to particles having the same area and size  $r_0 = 150$  nm, where  $r_0$  is the radius at  $c = 1$ . The same procedure was applied for scatterers with different sizes (see Tables S2 and S3 in the Supporting Information), and

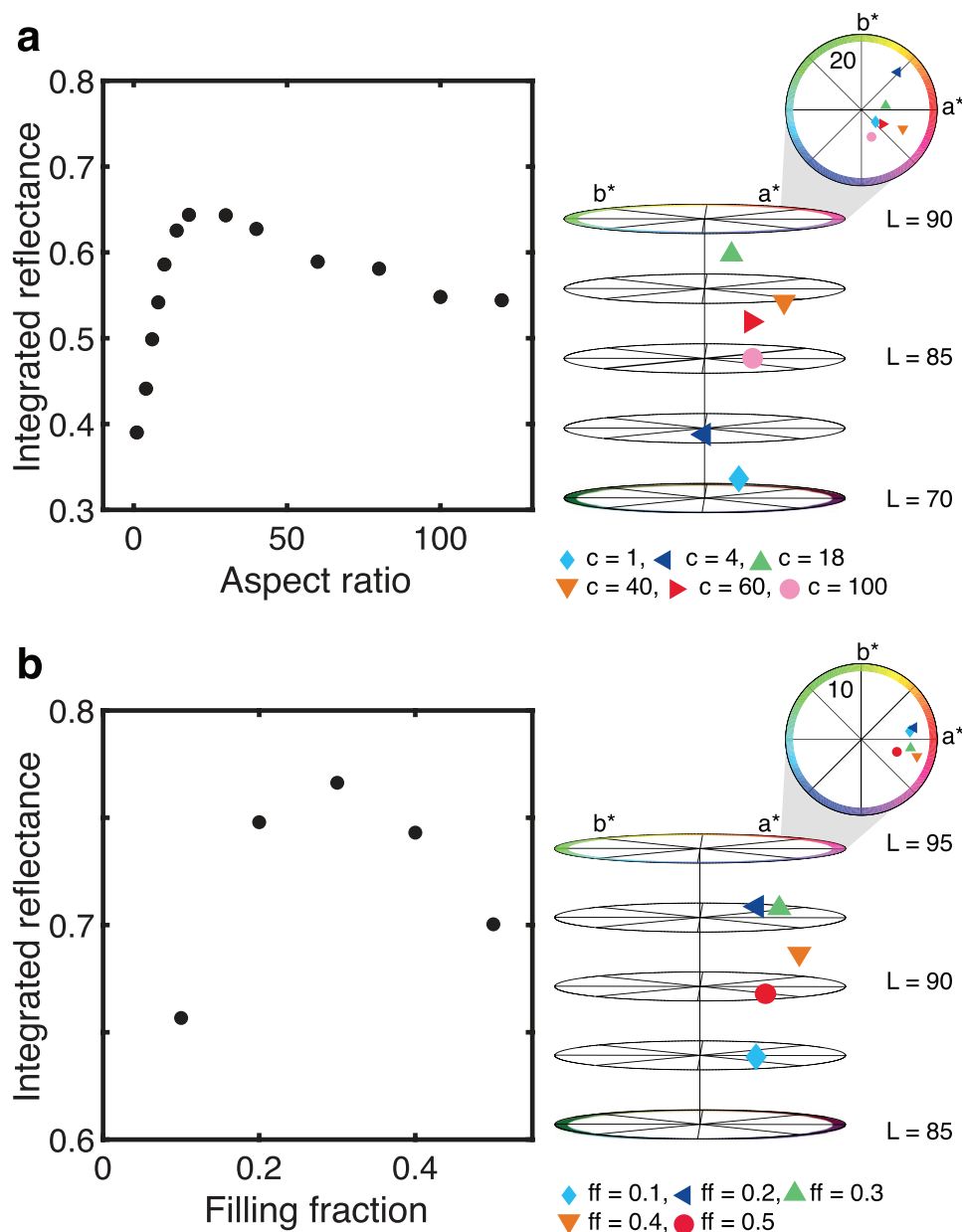


**Figure 3.** Simulated optical response for systems with different form anisotropy. Integrated reflectance over the visible range in function of the: a) aspect ratio of the particles for systems with  $ff = 0.1$ , and b) filling fraction of ensembles of scatters with  $c = 18$ . Insets: polar plot showing the CIELAB coordinates for different values of  $c$  and  $ff$  (panels (a) and (b), respectively). For all the simulations, the thickness of the systems was set to  $10 \mu\text{m}$ ,  $r_0 = 150$ , and  $n = 1.55$ .

their optimized values of  $c$  and  $ff$  are reported in Table 1 and Figure 1c (for  $n = 1.55$ ) and Table S1 and Figure S2a in the Supporting Information (for  $n = 2.60$ ).

Finally, the use of anisotropic particles adds an extra parameter in the scattering optimization problem: their degree of alignment. Analogous to the literature of liquid crystals, we define the director ( $\mathbf{n}$ ) as the average orientation of the particles (which in our framework is determined by the value of  $\theta$ ) and we quantify the degree of alignment by means of the order parameter ( $S$ )<sup>[44]</sup>

$$S = \left\langle \frac{3\cos^2\phi - 1}{2} \right\rangle \quad (4)$$

where  $\phi$  is the angle between the long axis of a given particle and  $\mathbf{n}$  and  $\langle \dots \rangle$  denote ensemble average. Following this definition,  $S = 1$  describes ensembles of particles perfectly aligned along  $\mathbf{n}$  (maximum anisotropy) and  $S = 0$  a completely random orientation (isotropic).

Figure 4 summarizes the role of the alignment of the particles on the scattering properties of a system. In detail, Figure 4a compares ensembles with different orientations of the director with respect to the incoming light. The integrated reflectance monotonically decreases as  $\theta$  increases, meaning that scattering is maximized for perpendicular orientation ( $\theta = 0$ ). In Figure 4b, the effect of the order parameter for fixed,

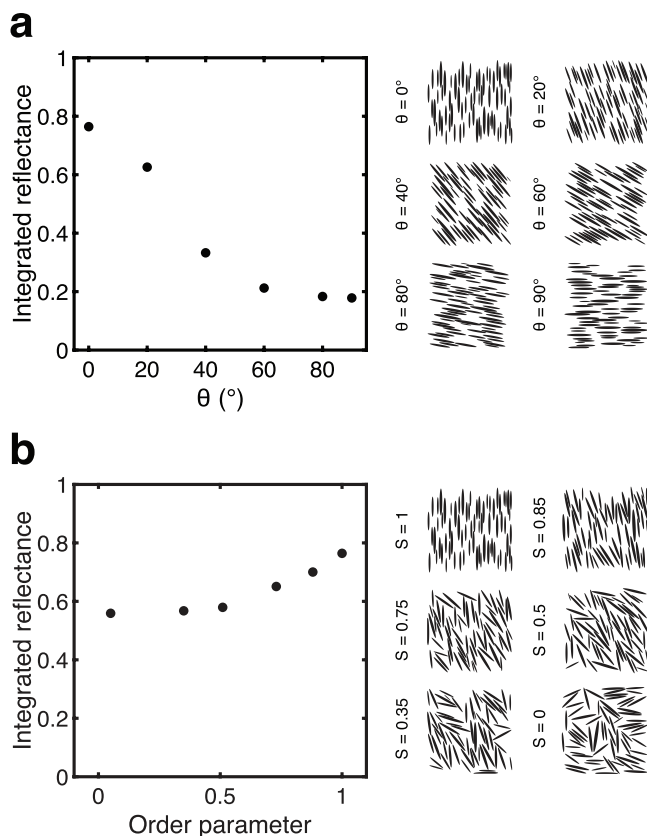


**Figure 4.** Simulated optical response for systems with different kinds and degrees of orientational, form, anisotropy. Integrated reflectance over the visible range in function of: a) the angle between the director and the direction perpendicular to the incoming beam ( $\theta$ ); the order parameter ( $S$ ). The amount of light reflected is maximized for particles oriented perpendicular to the incoming beam ( $\theta=0$ ) and with maximum orientational anisotropy ( $S=1$ ). For all the simulations, the thickness of the systems is  $10\ \mu\text{m}$ , the  $ff=0.3$ , and the particles have the same area, corresponding to  $r_0=150\ \text{nm}$ .

perpendicular orientation is reported. An increase in the order parameter leads to a larger integrated reflectance, implying that maximizing the degree of orientational anisotropy improves the scattering efficiency of a system.

### 3. Conclusions

In conclusion, we report a numerical study to disentangle the role of different types and degrees of anisotropy in the optical properties of a system. Our results show that using anisotropic particles aligned perpendicular to the exciting light ( $\theta = \sigma = 0$ ) increases the scattering efficiency of disordered systems, disregarding their structural correlations and refractive index. In particular, ensembles of anisotropic, low-refractive index, particles outperform those of their isotropic counterparts both in terms of reflectance (with 20% increase over the visible range) and of whiteness (90 against 84). This value of whiteness is comparable to the one for high-refractive index systems ( $n = 2.60$ ). In addition, for low-refractive index media, introducing anisotropic scattering elements decreases the amount

of material required to maximize scattering of 25%,  $ff = 0.3$  compared to  $ff = 0.4$  in the isotropic case.

The importance of these results is twofold: First, our numerical model explains why nature exploits anisotropic, aligned scatters to achieve lightweight, highly scattering structures. Second, our study proves the importance of anisotropy in maximizing the optical response of low-refractive index systems. This allowed us to unveil novel concepts to fabricate materials with a whiteness as high as the industrially available high-refractive index nanoparticles while being sustainable and biocompatible.

Our conclusions present the challenge of finding the correct fabrication procedure to manufacture materials that fulfill our indications.

### Supporting Information

Supporting Information is available from the Wiley Online Library or from the author.

### Acknowledgements

This work was supported in part by a BBSRC David Phillips Fellowship (BB/K014617/1), the European Research Council (ERC-2014-STG H2020 639088) to S.V. and G.J. and the Leverhulme Trusts Philip Leverhulme Prize and the Leverhulme Trust (No. RPG-2016-129) to J.B. G.J. thanks Dr. V. E. Johansen for assistance and counsel in setting the simulation setup, M. Bay for fruitful discussion on the colorspace representation, and Dr. L. Schertel for fruitful discussions.

### Conflict of Interest

The authors declare no conflict of interest.

### Keywords

disordered photonics, light-scattering optimization, scattering, sustainable materials, whiteness

Received: June 12, 2019

Revised: August 10, 2019

Published online:

- [1] P. Sheng, *Introduction to Wave Scattering, Localization and Mesoscopic Phenomena*, Springer, Berlin **1995**.
- [2] A. Ishimaru, *Wave Propagation and Scattering in Random Media, Vols. I and II*, Academic Press, San Diego, CA **1989**.
- [3] E. Akkermans, G. Montambaux, *Mesoscopic Physics of Electrons and Photons*, Cambridge University Press, Cambridge **2007**.
- [4] C. F. Bohren, D. R. Huffman, *Absorption and Scattering of Light by Small Particles*, Wiley, New York **2008**.
- [5] M. Florescu, S. Torquato, P. J. Steinhardt, *Proc. Natl. Acad. Sci. USA* **2009**, *106*, 20658.
- [6] S. F. Liew, J.-K. Yang, H. Noh, C. F. Schreck, E. R. Dufresne, C. S. O'Hern, H. Cao, *Phys. Rev. A* **2011**, *84*, 063818.
- [7] L. S. Froufe-Pérez, M. Engel, P. F. Damasceno, N. Muller, J. Haberkorn, S. C. Glotzer, F. Scheffold, *Phys. Rev. Lett.* **2016**, *117*, 053902.

- [8] G. M. Conley, M. Burrese, F. Pratesi, K. Vynck, D. S. Wiersma, *Phys. Rev. Lett.* **2014**, *112*, 143901.
- [9] L. S. Froufe-Pérez, M. Engel, J. Sáenz, F. Scheffold, *Proc. Natl. Acad. Sci. USA* **2017**, *114*, 9570.
- [10] S. Fraden, G. Maret, *Phys. Rev. Lett.* **1990**, *65*, 512.
- [11] L. F. Rojas-Ochoa, J. M. Mendez-Alcaraz, J. J. Sáenz, P. Schurtenberger, F. Scheffold, *Phys. Rev. Lett.* **2004**, *93*, 505.
- [12] G. J. Aubry, L. Schertel, M. Chen, H. Weyer, C. M. Aegerter, S. Polarz, H. Cölfen, G. Maret, *Phys. Rev. A* **2017**, *96*, 043871.
- [13] F. Riboli, F. Uccheddu, G. Monaco, N. Caselli, F. Intonti, M. Gurioli, S. E. Skipetrov, *Phys. Rev. Lett.* **2017**, *119*, 228.
- [14] P. D. García, P. Lodahl, *Ann. Phys.* **2017**, *529*, 1600351.
- [15] O. Leseur, R. Pierrat, R. Carminati, *Optica* **2016**, *3*, 763.
- [16] F. Bigourdan, R. Pierrat, R. Carminati, *Opt. Express* **2019**, *27*, 8666.
- [17] K. Vynck, M. Burrese, F. Riboli, D. S. Wiersma, *Nat. Mater.* **2012**, *11*, 1017.
- [18] F. Pratesi, M. Burrese, F. Riboli, K. Vynck, D. S. Wiersma, *Opt. Express* **2013**, *21*, A460.
- [19] M. Burrese, F. Pratesi, K. Vynck, M. Prasciolu, M. Tormen, D. S. Wiersma, *Opt. Express* **2013**, *21*, A268.
- [20] M. Burrese, F. Pratesi, F. Riboli, D. S. Wiersma, *Adv. Opt. Mater.* **2015**, *3*, 722.
- [21] L. Pattelli, A. Egel, U. Lemmer, D. Wiersma, *Optica* **2018**, *5*, 1037.
- [22] H. C. van de Hulst, *Light Scattering by Small Particles*, John Wiley and Sons, New York **1957**.
- [23] P. Vukusic, B. Hallam, J. Noyes, *Science* **2007**, *315*, 348.
- [24] M. Burrese, L. Cortese, L. Pattelli, M. Kolle, P. Vukusic, D. S. Wiersma, U. Steiner, S. Vignolini, *Sci. Rep.* **2014**, *4*, 1.
- [25] L. Cortese, L. Pattelli, F. Utel, S. Vignolini, M. Burrese, D. S. Wiersma, *Adv. Opt. Mater.* **2015**, *3*, 1337.
- [26] B. D. Wilts, X. Sheng, M. Holler, A. Diaz, M. Guizar-Sicairos, J. Raabe, R. Hoppe, S.-H. Liu, R. Langford, O. D. Onelli, D. Chen, S. Torquato, U. Steiner, C. G. Schroer, S. Vignolini, A. Sepe, *Adv. Mater.* **2018**, *30*, e1702057.
- [27] G. Jacucci, O. D. Onelli, A. De Luca, J. Bertolotti, R. Sapienza, S. Vignolini, *Interface Focus* **2019**, *9*, 20180050.
- [28] J. Syurik, G. Jacucci, O. D. Onelli, H. Hölscher, S. Vignolini, *Adv. Funct. Mater.* **2018**, *28*, 1706901.
- [29] M. S. Toivonen, O. D. Onelli, G. Jacucci, V. Lovikka, O. J. Rojas, O. Ikkala, S. Vignolini, *Adv. Mater.* **2018**, *30*, e1704050.
- [30] W. Zou, L. Pattelli, J. Guo, S. Yang, M. Yang, N. Zhao, J. Xu, D. S. Wiersma, *Adv. Funct. Mater.* **2019**, *29*, 1808885.
- [31] A. Weir, P. Westerhoff, L. Fabricius, K. Hristovski, N. von Goetz, *Environ. Sci. Technol.* **2012**, *46*, 2242.
- [32] S. Bettini, E. Boutet-Robinet, C. Cartier, C. Coméra, E. Gaultier, J. Dupuy, N. Naud, S. Taché, P. Grysan, S. Reguer, N. Thieriet, M. Réfrégiers, D. Thiaudière, J.-P. Cravedi, M. Carrière, J.-N. Audinot, F. H. Pierre, L. Guzylack-Piriou, E. Houdeau, *Sci. Rep.* **2017**, *7*, 40373.
- [33] H. L. Leertouwer, B. D. Wilts, D. G. Stavenga, *Opt. Express* **2011**, *19*, 24061.
- [34] J. R. DeVore, *J. Opt. Soc. Am.* **1951**, *41*, 416.
- [35] A. Koschan, M. A. Abidi, *Digital Color Image Processing*, Wiley-Interscience, Hoboken, NJ **2008**.
- [36] L. Brun, A. Trémeau, *Digital Color Imaging Handbook*, CRC Press, Boca Raton, FL **2002**.
- [37] A. Joiner, I. Hopkinson, Y. Deng, S. Westland, *J. Dent.* **2008**, *36*, 2.
- [38] H. Hottel, A. Sarofim, W. Dalzell, I. Vasalos, *AIAA J.* **1971**, *9*, 1895.
- [39] L. McNeil, R. French, *Acta Mater.* **2000**, *48*, 4571.
- [40] N. Elton, A. Legrix, *J. Coat. Technol. Res.* **2014**, *11*, 443.
- [41] L. Schertel, I. Wimmer, P. Besirske, C. M. Aegerter, G. Maret, S. Polarz, G. J. Aubry, *Phys. Rev. Mater.* **2019**, *3*, 015203.
- [42] J. Pendry, *Adv. Phys.* **1994**, *43*, 461.
- [43] M. Berry, S. Klein, *Eur. J. Phys.* **1996**, *18*, 226.
- [44] P. G. de Gennes, J. Prost, *The Physics of Liquid Crystals*, Oxford University Press, Oxford **1995**.